Plasma Phys. Control. Fusion **42** (2000) A139–A145. Printed in the UK PII: S0741-3335(00)11686-0

ELM phenomenon as an interaction between bootstrap-current driven peeling modes and pressure-driven ballooning modes

S Saarelma†, S Günter‡, T Kurki-Suonio† and H-P Zehrfeld‡

† Helsinki University of Technology, Euratom-TEKES Association, FIN-02015 HUT, Finland
‡ Max-Planck-Institut für Plasmaphysik, Boltzmannstraße 2, Garching, Germany

Received 29 September 1999

Abstract. An ELMy ASDEX Upgrade plasma equilibrium is reconstructed taking into account the bootstrap current. The peeling mode stability of the equilibrium is numerically analysed using the GATO [1] code, and it is found that the bootstrap current can drive the plasma peeling mode unstable. A high-n ballooning mode stability analysis of the equilibria revealed that, while destabilizing the peeling modes, the bootstrap current has a stabilizing effect on the ballooning modes. A combination of these two instabilities is a possible explanation for the type I ELM phenomenon. A triangularity scan showed that increasing triangularity stabilizes the peeling modes and can produce ELM-free periods observed in the experiments.

1. Introduction

ELMs (edge localized modes) are short bursts of particles and energy at the edge plasma, observed in H-mode (high confinement) plasmas. No steady-state H-mode has been achieved without ELMs. The type I ELMs investigated in this paper are detrimental to the divertor plates. On the other hand, ELMs can offer a way to improve particle circulation while sustaining a good heat confinement. All this makes the understanding the ELMs essential for future reactors. However, the ELM phenomenon has still eluded a solid physical model.

Connor *et al* [2] have proposed an ELM model for limited circular plasmas. In this model, the ELM cycle starts with the development of the edge pressure pedestal. The growth of the pedestal stops at the ballooning stability limit. Due to the pressure pedestal, the bootstrap current, which is proportional to the pressure and temperature gradients, starts to grow. Eventually, the bootstrap current destabilizes an ideal peeling mode causing an ELM crash and the loss of the edge pressure pedestal.

Since the ELMs occur at the edge, an accurate reconstruction of the plasma equilibrium at the edge is important when analysing this phenomenon. While small in the core plasma, the bootstrap current is significant at the edge. In particular, in the H-mode, where steep gradients exist near the separatrix, the bootstrap current cannot be ignored in the equilibrium reconstruction.

In this paper, the role of the bootstrap current on plasma stability is investigated and the proposed model for the ELMs is tested in realistic ASDEX Upgrade geometry using experimental plasma profiles. The role of the ballooning instability is also addressed. Finally, triangularity is studied as a means to control the ELMs.

2. Bootstrap current in equilibrium calculations

A standard free-boundary, separatrix-defined equilibrium is determined as a solution of

$$R^2\nabla\cdot\frac{\nabla\Psi}{R^2} = -2\pi\mu_0 R j_\mathrm{T} \tag{1}$$

where Ψ is the poloidal flux, and the toroidal component of the current density is given by

$$j_\mathrm{T} = \frac{\mu_0}{4\pi R}\frac{\mathrm{d}J^2}{\mathrm{d}\Psi} + 2\pi R\frac{\mathrm{d}p}{\mathrm{d}\Psi} \tag{2}$$

Here J is the poloidal current and p the plasma pressure.

The standard way of calculating a plasma equilibrium is to prescribe functions $\mathrm{d}J^2/\mathrm{d}\Psi$ and $\mathrm{d}p/\mathrm{d}\Psi$ and to solve the Poisson problem (1). Usually, it is possible to obtain the function $\mathrm{d}p/\mathrm{d}\Psi$ from the experiments, but the poloidal current function is not known. Therefore, some assumptions about the $\mathrm{d}J^2/\mathrm{d}\Psi$ term have to be made. If the bootstrap current can be ignored, the poloidal current profile is independent of the temperature and pressure profiles. However, at the plasma edge, where the gradients and the bootstrap current are large, this assumption is not valid.

An equilibrium including bootstrap current can be solved from equation (1) by conceiving $\mathrm{d}J^2 = \mathrm{d}\Psi$ as expressed by the flux surface-average $\langle \boldsymbol{j}\cdot\boldsymbol{B}\rangle$. Starting from the definition of the magnetic field, Ampère's law, and equation (1), it is possible to derive an expression

$$\langle \boldsymbol{j}\cdot\boldsymbol{B}\rangle = \langle B^2\rangle\frac{\mathrm{d}J}{\mathrm{d}\Psi} + \mu_0 J\frac{\mathrm{d}p}{\mathrm{d}\Psi} \qquad \langle \boldsymbol{j}\cdot\boldsymbol{B}\rangle = \int\int \boldsymbol{j}\cdot\boldsymbol{B}\langle \boldsymbol{j}\cdot\boldsymbol{B}\rangle\frac{\mathrm{d}S}{|\nabla V|}. \tag{3}$$

Here, the surface-averaged magnetic field $\langle B^2\rangle$ and its components are

$$\langle B^2\rangle = \mu_0(L_\mathrm{P}J^2 + L_\mathrm{T}I^2) \qquad \langle B_\mathrm{T}\rangle = \mu_0 L_\mathrm{P}J^2 \qquad \langle B_\mathrm{P}^2\rangle = \mu_0 L_\mathrm{T}I^2 \tag{4}$$

where I is the toroidal current, and L_P and L_T are the inductance coefficients

$$L_\mathrm{P} \equiv \frac{\mu_0}{4\pi^2}\langle 1/R^2\rangle \qquad L_\mathrm{T} \equiv \frac{4\pi^2\mu_0}{\langle |\nabla V|^2/R^2\rangle}. \tag{5}$$

Using (3), the expression $\mathrm{d}J/\mathrm{d}\Psi$ can be eliminated from the (2) and we obtain

$$j_\mathrm{T} = 2\pi R\left\{\frac{B_\mathrm{T}^2}{\langle B^2\rangle}\frac{\langle \boldsymbol{j}\cdot\boldsymbol{B}\rangle}{\mu_0 J} + \left(1 - \frac{B_\mathrm{T}^2}{\langle B^2\rangle}\right)\frac{\mathrm{d}p}{\mathrm{d}\Psi}\right\}. \tag{6}$$

We have thus eliminated $\mathrm{d}J/\mathrm{d}\Psi$ from the expression for j_T. However, j_T still depends on J itself as well as on the toroidal current I. They can be solved, if $\langle \boldsymbol{j}\cdot\boldsymbol{B}\rangle/\mu_0 J$ is given. Taking the flux surface average of (1) and using (3), we can derive two ordinary differential equations for I and J:

$$\frac{\mathrm{d}I}{\mathrm{d}V} = \frac{\langle B_\mathrm{T}^2\rangle}{\langle B^2\rangle}\frac{\langle \boldsymbol{j}\cdot\boldsymbol{B}\rangle}{\mu_o J} + \left(1 - \frac{\langle B_\mathrm{T}^2\rangle}{\langle B^2\rangle}\right)\frac{\mathrm{d}p}{\mathrm{d}\Psi} \tag{7}$$

$$\frac{1}{2}\frac{\mathrm{d}J^2}{\mathrm{d}V} = L_\mathrm{R} I\frac{\langle B_\mathrm{T}^2\rangle}{\langle B^2\rangle}\left\{-\frac{\langle \boldsymbol{j}\cdot\boldsymbol{B}\rangle}{\mu_0 J} + \frac{\mathrm{d}p}{\mathrm{d}\Psi}\right\}. \tag{8}$$

Here L_R is a ratio of inductances $L_\mathrm{T}/L_\mathrm{P}$.

Let us now consider the functions $\langle \boldsymbol{j}\cdot\boldsymbol{B}\rangle/\mu_0 J$ and $\mathrm{d}p/\mathrm{d}\Psi$ as given and $\langle B^2\rangle$ as described by equation (4). The solution of the subsequent nonlinear two-point boundary value problem described by (7) and (8) leads to a complete determination of the right-hand side for the Poisson problem (1): we prescribe $I = 0$ on the magnetic axis and $J^2 = J_\mathrm{p}^2$ at the plasma boundary, and solve for I and J^2. The solution for J^2 can be used for the calculation of the current density according to (2). If the total plasma current I_p is prescribed, we have more boundary

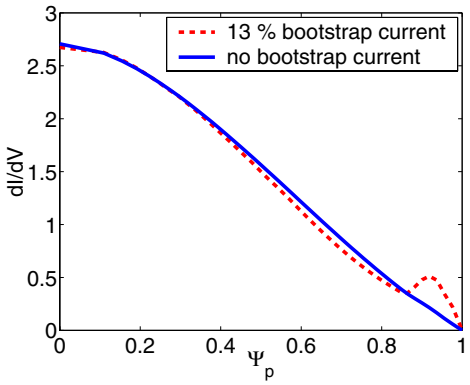

Figure 1. Toroidal current density distribution of an equilibrium with no bootstrap current (full curve) and if the bootstrap current amounts to 13% of the total current (dashed curve).

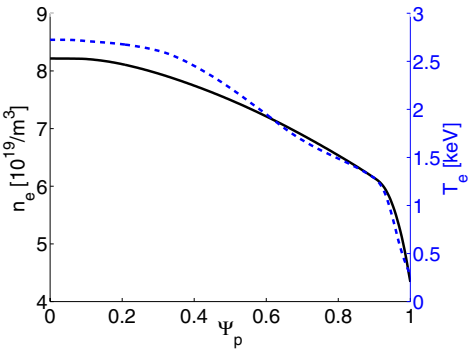

Figure 2. Fitted electron temperature (dashed curve) and density (full curve) profiles used in the equilibrium reconstruction. The ion temperature is assumed to be the same as the electron temperature.

conditions than dependent variables, and therefore need one additional free parameter C_s in $\langle \boldsymbol{j}\cdot\boldsymbol{B}\rangle = \langle \boldsymbol{j}\cdot\boldsymbol{B}\rangle(C_s)$. Here, C_s represents the part of $\langle \boldsymbol{j}\cdot\boldsymbol{B}\rangle$ that contributes to the equilibrium through I and J (equations (7) and (8)). The equations (7) and (8) can be augmented by

$$\frac{\mathrm{d}C_s}{\mathrm{d}V} = 0 \tag{9}$$

so that we now have three variables and three boundary conditions.

In order to get the plasma equilibrium, we now need to prescribe only the flux surface-averaged parallel current and the pressure gradient instead of $\mathrm{d}J^2/\mathrm{d}\Psi$. This makes the bootstrap current equilibrium reconstruction possible. Part of the parallel current is due to the inductively driven current $\langle \boldsymbol{j}\cdot\boldsymbol{B}\rangle_{\mathrm{CD}}/\mu_0 J$. In addition, it is possible to derive an analytical expression for the bootstrap current $\langle \boldsymbol{j}\cdot\boldsymbol{B}\rangle_{\mathrm{bs}}/\mu_0 J$ which depends only on the pressure and temperature gradients and, thus, can be obtained from the experiments. Three models with slightly different assumptions on the geometry and the collisionality were considered (the Hirshman model and the Harris model in [3], and the Wilson model in [4]). It was found that the differences between the results from different models were small. In the numerical studies presented in this paper, the Wilson model was used:

$$\langle \boldsymbol{j}\cdot\boldsymbol{B}\rangle_{\mathrm{bs}} = \frac{p_e R B_T x}{D}\left(c_1\frac{1}{p_e}\frac{\mathrm{d}p_e}{\mathrm{d}\psi} + c_2\frac{1}{p_i}\frac{\mathrm{d}p_i}{\mathrm{d}\psi} + c_3\frac{1}{T_e}\frac{\mathrm{d}T_e}{\mathrm{d}\psi} + c_4\frac{1}{T_i}\frac{\mathrm{d}T_i}{\mathrm{d}\psi}\right) \tag{10}$$

with

$$\begin{aligned}
c_1 &= \frac{4.0 + 2.6x}{(1.0 + 1.02\nu_{*e}^{0.5} + 1.07\nu_{*e})(1.0 + 1.07\epsilon^{1.5}\nu_{*e})}\\
c_2 &= \frac{T_i}{T_e}c_1\\
c_3 &= \frac{7.0 + 6.5x}{(1.0 + 0.57\nu_{*e}^{0.5} + 0.61\nu_{*e})(1.0 + 0.61\epsilon^{1.5}\nu_{*e})}\\
c_4 &= \left(\frac{-1.17/(1 + 0.46x) + 0.35\nu_{*i}^{0.5}}{1.0 + 0.70\nu_{*i}^{0.5}} + 2.10\nu_{*i}^2\epsilon^3\right)\frac{1}{(1.0 + \nu_{*i}^2\epsilon^3)(1.0 + \nu_{*e}^2\epsilon^3)}\\
D &= 2.4 + 5.4x + 2.6x^2
\end{aligned} \tag{11}$$

where x is the trapped particle fraction ($\approx 1.46\sqrt{\epsilon}$), ν_{*j} is the collisionality of the particle type j and ϵ is the inverse aspect ratio (a/R).

Figure 1 shows poloidal current density peaking at the edge as the bootstrap fraction of the total current is increased. The inductively driven current profile was fixed so that the equilibrium reconstruction gave q-profiles that agreed with experimental measurements as closely as possible.

3. Peeling mode stability

Peeling modes are ideal current-driven MHD instabilities that are localized at the plasma edge. Consequently, their stability depends on the current profile at the edge, which makes the bootstrap current important in the stability analysis.

An ASDEX Upgrade ($R = 1.6$ m, $a = 0.5$ m) shot (shot No 11991) with type I ELMs was analysed using the ideal MHD stability code GATO. Temperature and density profiles were taken from the experiment and smoothed (figure 2), and the bootstrap current was included in the equilibrium reconstruction as described above. For the stability analysis, the q-value on axis was fixed slightly above one for all cases.

It was found that increasing the fraction of the bootstrap current caused plasma to become peeling mode unstable (figure 3). For realistic values of bootstrap current, toroidal mode numbers ranging from 3 to 6 were found unstable. In the figure, the $n = 2$ mode seems marginally unstable, but the small value of the growth rate is at the limit of the numerical resolution of the GATO code and it can be ignored. Only at very high values of bootstrap current fraction does the $n = 2$ mode become really unstable. The unstable mode numbers agree with the Mirnov coil observations of the type I ELM precursors [5]. Similar results were obtained at DIII-D for peeling modes associated with ELMs [6].

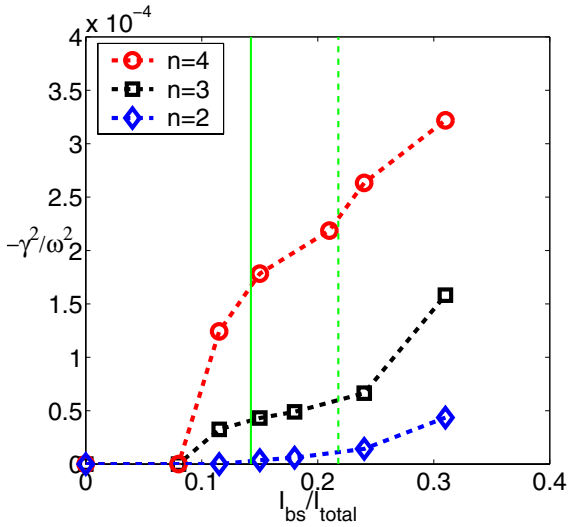

Figure 3. Peeling mode growth rates for three toroidal mode numbers ($n = 1$ is stable in the whole range). The vertical lines represent calculated bootstrap currents by two alternative methods (analytical, using $C_s = 1$ in equation (9) (full line) and transport calculations with the ASTRA [7] code (dashed line). ASTRA uses the Hirshman model for bootstrap current calculations).

4. Ballooning mode stability

The GATO analysis also revealed that the instability had a ballooning component. Using the ballooning code GARBO [8], the tested equilibria were found to be high-n ballooning unstable (figure 4). GARBO calculates the threshold pressure gradient for ballooning instability and compares it with the experimental pressure gradient. Only low toroidal mode numbers ($n < 7$) can be accurately identified experimentally in ASDEX Upgrade. Therefore, the high n-modes cannot be distinguished in the precursors and a comparison with the numerical results is difficult.

It is possible that, since the profiles were created with a slightly pessimistic assumption (e.g. the T_i pedestal is as steep as the T_e pedestal), the ballooning instability is due to an unrealistically steep pressure gradient. However, the peeling instability is current driven, and the uncertainty in the pressure profile does not affect it as much. Therefore, even if the bootstrap current is slightly lowered due to the decrease in the pressure and temperature gradients, the results presented in the previous section are still valid. The curves in figure 3 would only move slightly to the right.

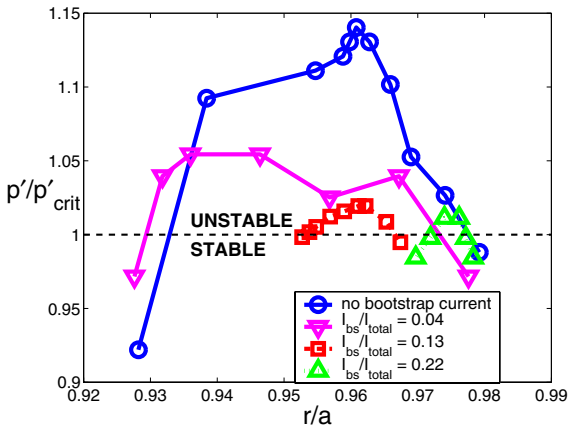

Figure 4. High-n ballooning stability for shot No 11991 at 2.0 s for different bootstrap fractions. Only the most unstable part is plotted. Other parts of the plasmas are stable. p'_{crit} is the threshold pressure gradient for ballooning instability.

The ballooning analysis also revealed that, as the bootstrap current fraction is increased, the stability improves. In figure 4 the stability of a plasma both without a bootstrap current and with 4%, 13%, and 22% bootstrap current fractions are compared. Clearly, while the bootstrap current has a destabilizing effect on the peeling modes, it stabilizes the ballooning modes. The reason for the stabilizing effect is that, since we are investigating the edge of a strongly shaped plasma, the decreasing shear (caused by the bootstrap current) may open a second stability access.

5. Test case: triangularity

Two ASDEX Upgrade shots (shot No 11991 and shot No 11795) with similar plasma profiles but with differing plasma shapes (figure 5) were analysed with respect to the peeling modes. In addition to these, very high triangularity was investigated using experimental plasma profiles (T, n), but adjusting the plasma shape to a much higher value of triangularity. The q-profiles of

the two experimental cases are almost identical ($q_{95} = 3.65$ for shot No 11991 and $q_{95} = 3.85$ for shot No 11795). For the very high triangularity case, $q_{95} = 4.4$. It was found that increasing the plasma triangularity stabilizes the plasma (figure 6). This agrees with the experimental observations: long ELM-free periods have been detected in high triangularity ($\delta = 0.3$–0.4) but not with low ($\delta = 0.1$–0.2) or medium triangularity ($\delta = 0.2$–0.3) [9]. ELM frequencies are also lower in the high triangularity shots.

Increased triangularity had very small effect on the ballooning stability. The bootstrap current fraction scan for the ballooning stability of shot No 11795 was almost identical to that of shot No 11991. The differences in the stability for most bootstrap current fractions were less than 1%. Only for a high bootstrap current fraction (22%) was the ballooning stability of the high triangularity shot (shot No 11795) better.

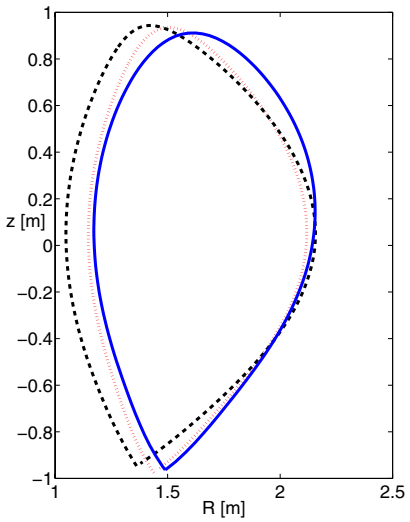

Figure 5. Triangularity variation from $\delta = 0.24$ (shot No 11991, full curve) to $\delta = 0.34$ (shot No 11795, dotted curve). The dashed curve represents a discharge with extreme triangularity. It was composed from shot No 11991 equilibrium by increasing its triangularity artificially.

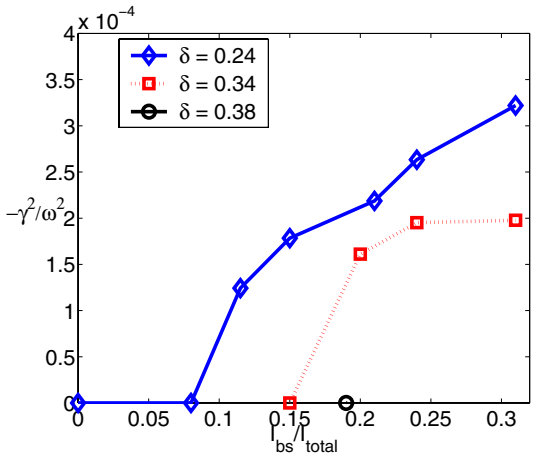

Figure 6. Growth rates of the $n = 4$ peeling mode for medium ($\delta = 0.24$) and high ($\delta = 0.34$) triangularity. The extra data point ($\delta = 0.38$) represents an artificial equilibrium with extreme triangularity.

6. Discussion

Unstable peeling modes were found for equilibria with a high bootstrap current fraction. Neglecting the bootstrap current, the same plasma was found to be high-n ballooning unstable. Increasing the bootstrap current fraction made the plasma marginally ballooning stable. So, while destabilizing the peeling modes, the bootstrap current can improve the ballooning stability by modifying the shear near the edge and possibly giving access to the second stability region.

These numerical results calculated for realistic ASDEX Upgrade profiles and geometry support the Connor model for type I ELMs that was created for circular limited plasmas. Based on the numerical analysis of the instabilities, the Connor model appears feasible for shaped plasmas as well. The plasma is at the ballooning stability boundary and the increasing bootstrap current eventually drives the plasma peeling mode unstable. While the actual time

sequence of the events remains unresolved, the analysis shows that both components (peeling and ballooning) are present.

The plasma triangularity was found to have a stabilizing effect on the peeling modes (higher bootstrap fraction was needed to drive the plasma unstable). The triangularity effect on the ballooning stability was found to be negligible in the two shots that were analysed. The increased stability agrees with the experimental observations and supports the proposition that type I ELMs are triggered by the peeling mode instability.

References

[1] Bernard L C, Helton F J and Moore R W 1981 *Comput. Phys. Commun.* **24** 377
[2] Connor J W, Hastie R J and Wilson H R 1997 MHD stability of the tokamak edge *UKAEA Report* FUS 383
[3] Kessel C 1994 *Nucl. Fusion* **34** 1221
[4] Wilson H R 1994 *UKAEA Report* FUS 271
[5] Marascheck M, Günter S, Kass T, Saarelma S, Zehrfeld H P and Zohm H 1998 MHD characteristics of ELMs and their precursors *Proc. 25th EPS Conf. on Controlled Fusion (Prague, 1998)* 492
[6] Turnbull A D, Osborne T H, Strait E J, Lao L L, Miller R L and Taylor T S1998 Identification of intermediate *n* ideal MHD kink-peeling modes with ELMs in DIII-D H-mode discharges *Bull. Am. Phys. Soc.* **43** 1761
[7] Pereverzev G V *et al* 1991 ASTRA an automatic system for transport analysis in a tokamak *IPP Report* 5/42, MPI f. Plasmaphysik, Garching
[8] Zehrfeld H P 1998 Equilibrium and ballooning stability of resistive tokamak plasmas near the separatrix *Proc. 25th EPS Conf. on Controlled Fusion (Prague, 1998)* p 1927
[9] Suttrop W *et al* 2000 Effect of plasma shape variation on H-mode pedestal properties and edge localized modes in ASDEX upgrade *Plasma Phys. Control Fusion* **42** A97